symmetry

MDPI

Article

Numerical Investigation of the Savonius Vertical Axis Wind Turbine and Evaluation of the Effect of the Overlap Parameter in Both Horizontal and Vertical Directions on Its Performance

Mohammad Ebrahimpour [1], Rouzbeh Shafaghat [1,*], Rezvan Alamian [1] and Mostafa Safdari Shadloo [2]

[1] Sea-Based Energy Research Group, Babol Noshirvani University of Technology, 47148 Babol, Iran; m.ebrahimpour.0123@gmail.com (M.E.); ralamian@nit.ac.ir (R.A.)

[2] CORIA Lab./CNRS, University and INSA of Rouen, 76000 Rouen, France; msshadloo@coria.fr

* Correspondence: rshafaghat@nit.ac.ir; Tel.: +98-(11)-3233-2071-1333; Fax: +98-(11)-3231-0968

Received: 28 May 2019; Accepted: 19 June 2019; Published: 21 June 2019

Abstract: Exploiting wind energy, which is a complex process in urban areas, requires turbines suitable for unfavorable weather conditions, in order to trap the wind from different directions; Savonius turbines are suitable for these conditions. In this paper, the effect of overlap ratios and the position of blades on a vertical axis wind turbine is comprehensively investigated and analyzed. For this purpose, two positive and negative overlap situations are first defined along the X-axis and examined at the different tip speed ratios of the blade, while maintaining the size of the external diameter of the rotor, to find the optimum point; then, the same procedure is done along the Y-axis. The finite volume method is used to solve the computational fluid dynamics. Two-dimensional numerical simulations are performed using URANS equations and the sliding mesh method. The turbulence model employed is a realizable K-ε model. According to the values of the dynamic torque and power coefficient, while investigating horizontal and vertical overlaps along the X- and Y-axis, the blades with overlap ratios of HOLR = +0.15 and VOLR = +0.1 show better performances when compared to other corresponding overlaps. Accordingly, the average C_m and C_p improvements are 16% and 7.5%, respectively, compared to the base with a zero overlap ratio.

Keywords: Savonius vertical axis wind turbine; horizontal overlap ratio; vertical overlap ratio; torque coefficient; power coefficient

1. Introduction

The increasing need for energy and the reduction of fossil fuel resources on one hand, and the strict laws on the environment and global warming on the other hand, draw governments' attention to renewable energy resources [1–3]. According to recent reports, the global use of energy by 2015 based on fossil, nuclear, and renewable energy resources were 78.4%, 2.3%, and 19.3%, respectively [4].

Renewable energy that includes wind, solar, geothermal, marine, biomass, and hydropower energy, seems to be the best alternative to humankind's exceedingly growing energy consumption and replacing of fossil sources [5]. Among others, wind energy is considered the least costly source of available renewable energy and is growing at a very fast pace. Since 1996, the capacity to generate energy from wind power has grown significantly as one of the most important renewable energy sources in the world today. The pioneers of this route are developed countries such as China, the United States, and Germany. The total wind energy capacity at the end of 2016 was about 487 gigawatts and is expected to reach 2000 gigawatts by 2030.

In the wind energy industry, there are two main types of wind turbines: horizontal axis wind turbines (HAWT) and vertical axis wind turbines (VAWT). In general, the efficiency of horizontal axis turbines is better than that of vertical axis turbines in wind power extraction (Figure 1). Therefore, most wind turbines in the commercial market today are horizontal axis turbines.

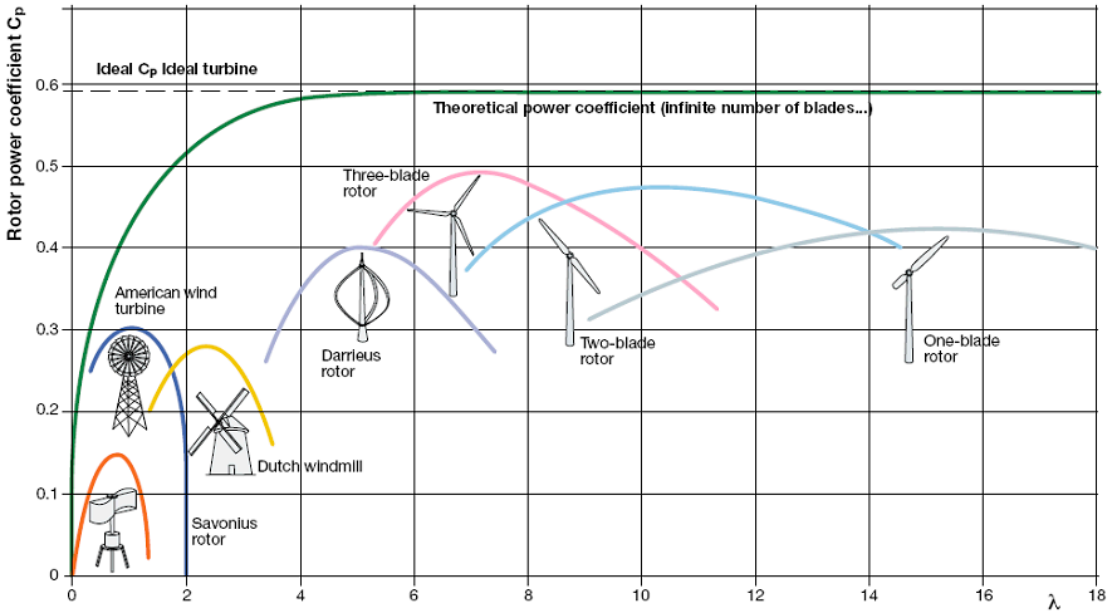

Figure 1. The variation curve of the rotor power coefficient (Cp) average to tip speed ratio (TSR) in different types of wind turbines [6].

Vertical axis wind turbines (VAWTs) represent a much less employed type of wind turbine. However, new trends in the use of VAWT technologies presented by researchers and manufacturers, as well as their benefits, have led to significant recent developments [7]. In some cases, these turbines have advantages over the horizontal ones, including a lack of dependence on the wind direction, easier maintenance, less visual impact, less noise pollution, and a better performance under skewed wind conditions. Urban winds include disordered, indirect, and transverse flows due to the existence of many obstacles (i.e., buildings). For this reason, VAWTs are more suitable than horizontal axis turbines for urban conditions [8]. VAWTs are made in various shapes. The two main types are lift-type turbines (Darrieus) and drag-type turbines (Savonius). Lift-type turbines are designed for high speeds and low torque and require an external or manual force to start working. Drag-type turbines are designed for low speeds and high torque. For conditions with turbulent flows and storms and whenever reliability and cost are more important than productivity, the latter turbines are the best option. This is because, unlike the Darrieus turbine, they do not need external forces to start working.

Numerical studies on renewable energy are very common [9–11]. The purpose of the present work is to conduct a numerical study of a particular type of drag-type wind turbine, called the conventional semi-circular Savonius rotor. In simulations, different turbulence models such as DNS, LES and RANS are used according to the required accuracy. The highest accuracy is expected from the DNS model [12,13], which has a high computational cost. However, the present article chose the RANS model due to the available facilities. The airflow around these turbines has a turbulent and transient nature, for which, in the present paper, the finite volume method is used for analysis. The general concept of drag-type turbines was established based on the developed principles of the Feltner model [14]. In recent years, various studies have been done to improve their performance. In 2015, Fredericks et al. [15] examined the impact of the number of blades on the efficiency of the Savonius turbine using empirical and numerical studies. They found that a four-blade turbine is more effective for a low tip speed ratio, while for a high tip speed ratio, a turbine with three blades is more

efficient. Roy and Saha [16] experimentally compared a turbine with a novel geometry with four previous models, claiming an increase in its efficiency compared to the standard Savonius turbine. Tahani et al. [17] simulated five three-dimensional rotor models, including a Savonius with a simple circular blade, twisted Savonius with a simple circular blade, Savonius with a simple circular blade and variable cut plane, twisted Savonius with a simple circular blade and variable cut plane, and Savonius with two or three blades and a conical shaft. They examined the effect of different parameters such as rotor height and power coefficient to eventually find the optimal conditions for these turbines. Lee et al. [18] investigated the functional characteristics and shape of the helical Savonius turbine, with varying twist angles, and calculated the power and torque coefficients for different azimuth angles, both numerically and experimentally. Additionally, the highest power coefficient was obtained at a 45 degree twist angle. This value was calculated as 0.13. Roy et al. [19] investigated the height, diameter, and aspect ratio of the semicircular-bladed Savonius style wind turbine using a differential evolution-based inverse optimization methodology and performed optimization by reducing the space occupied by the rotor, and the overall dimensions were reduced by up to 9.8%. Wang and Zhan [20] compared three models of helical, semi-cylindrical, and semicircular Savonius turbines by investigating the effect of rotor height and twist angle, with respect to the parameter of the output dynamic torque, as well as the urban aesthetic theme. The simulations were carried out three-dimensionally by the sliding mesh method using the RANS equation and turbulence realizable k-ε model via the SIMPLE algorithm for the pressure-speed coupling. Müller et al. [21] experimentally tested the Persian or Sistan wind mill, which is the oldest wind energy device. The efficiency of this machine was assumed to be between 5 and 14%. A series of tests were conducted with a six-bladed model of a 0.6 m diameter and 0.5 m high runner. Two geometries were investigated: with an open downstream side and with a closed downstream side. The second geometry showed a better performance. It was found that a gap between the blades and axis of approximately 1/6 of the blade width is essential and with minimum torque applied, blade velocities can reach up to 2.5 times the wind speed. Roy and Saha [22] performed two-dimensional simulations using the k-ε model under the influence of the wall function and the SIMPLE algorithm in order to investigate the overlap ratios in conventional Savonius wind turbines. They acknowledged that these turbines would have a better efficiency at the overlap ratio of 0.2. Mohammad et al. [23] compared the results of a two-dimensional simulation for turbulent models SST k-ω, RSM, standard k-ε, and realizable k-ε to optimize the conventional Savonius turbines. They found that the realizable k-ε model exhibited the smallest error when compared to Hayashi's [24] experimental data by considering the uncertainty errors. This is an important part of experimental works. A detailed review of this topic was completed by Rizzo and Caracoglia [25], where wind-tunnel experimental errors, associated with the measurement of aeroelastic coefficients of bridge decks, was explored, and expressed no unexpected large irregularity, potentially linked to a systematic error. Tian et al. [26] used a BANKI wind rotor on the medians of the highway to recover energy from the wake of vehicles on both sides of the highway. To evaluate the performance of the rotor, 3D computational fluid dynamics simulations were performed. Five typical situations, including one car on the passing lane, one bus on the passing lane, two opposite moving cars on the passing lane, one car on the fast main lane, and one bus on the fast main lane, were considered and studied. The SST k-ω was used to model the turbulence terms of the RANS equations. The results showed that (1) the highest power coefficient of 0.00464 occurs from the wake of a bus on the passing lane, (2) the maximum power coefficient of two opposite moving cars on the passing lane is a little (7.5%) higher than the power coefficient of one car on the passing lane, (3) the rotor exerts negligible influences on the forces of the vehicles, and (4) the rotor cannot generate power from vehicles on the fast main lane because of the large distance between the rotor and the vehicle. Krzysztof Rogowski [27] analyzed the flow around a one-bladed Darrieus-type wind turbine numerically, by employing a laminar model and two SST k-ω and RNG k-ε turbulence models, and showed that the RNG k-ε turbulence model has a good precision in computing aerodynamic blade loads for the up- and downwind parts of the rotor. The laminar model and the SST k-ω turbulence model a bit more than the tangential aerodynamic blade loads at the downwind

part of the rotor. Ferrari et al. [28] simulated the dynamic of a conventional Savonius wind turbine two- and three-dimensionally at different wind speeds and different angular velocities using Open FOAM software. They calculated the values of lift, drag, power, and torque coefficients, and compared the error values and differences between them. To do this, they evaluated three models of one and two equations of Spalart–Allmaras, realizable k-ε, and SST k-ω, among which the highest sensitivity was determined for SST k-ω; therefore, they applied this method. Jin et al. [29] examined the effect of different barrier plate parameters on the upstream flow, including the height, width, and distance of rotors, to evaluate the performance of vertical axis wind turbines. The simulation results were compared to experimental data with and without using the deflector, which showed a good fit. To do this, the SST k-ω and realizable k-ε models were compared with the experimental result and they stated that the SST k-ω model had positive characteristics of the k-ω method for the internal parts of the boundary layer. Simultaneously, this model operated in a free flow in the same way as the k-ε model and did not have the problems of the k-ω model. In sum, they stated that the results obtained by solving the SST k-ω method were more accurate than those of the k-ε model.

As can be seen from the literature, the change in geometry has a significant effect on wind turbine efficiency. However, the effects of overlap distance between the blades of Savonius-type turbines, in two directions of the rotor's cross section, which can be used to achieve the optimal placement of blades relative to each other, have not yet been considered to the authors' best knowledge. Therefore, in the present work, the main parameter that is used to optimize the performance of VAWT of the Savonius-type is the overlap distance between two blades. The work that has been done in relation to overlap ratios has presented different results, from 0.15 to 0.25 overlap ratios [22,30,31]. Fujisawa [30] carried out surveys by measuring the pressure distribution in the blade and monitoring the flow of fluid in and around the rotating and non-rotating rotors. The experiments were performed on four rotors with a half-diameter blade and an overlap ratio of 0 to 0.5. Increasing the overlap ratio, especially in the return mode, showed a better static torque recovery, and the maximum torque and rotor power were obtained at the overlap ratio of 0.15. Alom et al. [32] performed two-dimensional simulations using the SST k-ω model in order to investigate the overlap ratios in an elliptical-bladed Savonius wind turbine. They acknowledged that an elliptical-bladed rotor with a 0.15 overlap ratio exhibited the highest performance relative to the other overlap ratios, in the range of 0 to 0.3. Kumbernuss et al. [31] examined the overlap ratios of 0, 0.16, and 0.32, and the angular changes of phases 0, 15, 30, 45, and 60 degrees between two stages in the Savonius turbine. Experiments were carried out at various wind speeds. The best power coefficients were reported for the overlap ratios of 0 and 0.32 at a phase change angle equal to 60 degrees, and for the overlap ratio of 0.16, at a phase change angle equal to 30 degrees. In the present work, the geometric parameter of the overlap distance was also investigated. The difference between this and previous work is that it is employed to examine the overlap ratio as positive and negative in comparison to the base state without overlap. For this purpose, the overlaps were performed along both the X- and Y-axes, in both positive and negative directions. To illustrate the process, a guideline was selected on one of the blades and this point was denoted as the reference. In the optimal overlapping process, in the first step, the guide point is changed in the X-axis to reach an optimal point. Then, at the optimum point, the overlaps are checked along the Y-axis to eventually reach an optimal point.

2. Subject Theory

The overlap distance is the region between the two blades in the Savonius turbine. This distance is used to compensate for the differential pressures in the concave and convex sections in the leading blade. The overlap ratio in different papers is sometimes defined slightly differently, but, in general, it expresses a common concept that Roy and Saha described in their article as the relation (1) [33]:

$$Overlap\ Ratio = {}^{e}/_{d} \quad (1)$$

where d is the chord of the blade and e is the overlap distance between the two blades (Figure 2).

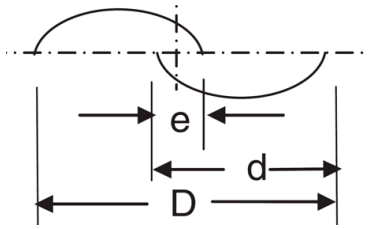

Figure 2. Schematic diagram of the overlap ratio according to Roy and Saha [33].

The difference between the current study and previous ones in the field of the overlap ratio is that the overlap ratio is defined as positive and negative values considering the base state with zero overlap. For this purpose, overlaps are performed along both the X- and Y-axes. To explain the process, a Guide Point (GP) is defined, which is located on the inner end of one of the blades marked with a cross sign in Figure 3. The process of achieving optimal overlap is as follows: in the first step, the GP is displaced on the X-axis, and the coordinates of these displaced points change as GP (x, 0). Here, x is the horizontal variable while keeping the vertical overlap zero. Then, at the optimal point obtained in the previous step, the overlaps in the direction of the Y-axis are checked and the GP moves on (C, y), where y is the vertical variable while keeping C as the optimum constant point obtained in the previous step. In this way, the optimum position of the blades in a region with a constant swept area is obtained for different dimensions and positions of the blade. The overlap ratios defined in the present work are as follows:

Horizontal overlap ratio:

$$HOLR = e_1/R \tag{2}$$

Vertical overlap ratio:

$$VOLR = e_2/R \tag{3}$$

Depending on the placement of the GP, each of the overlap ratios may get a positive or negative value. This means that if the GP is located in the negative region of the X-axis, the horizontal overlap is a negative amount, and if it is located in the positive region of the X-axis, the horizontal overlap is a positive amount. Similarly, if the GP is located in the negative region of the Y-axis, the vertical overlap is a negative amount, and if it is located in the positive region of the Y-axis, the vertical overlap is a positive amount.

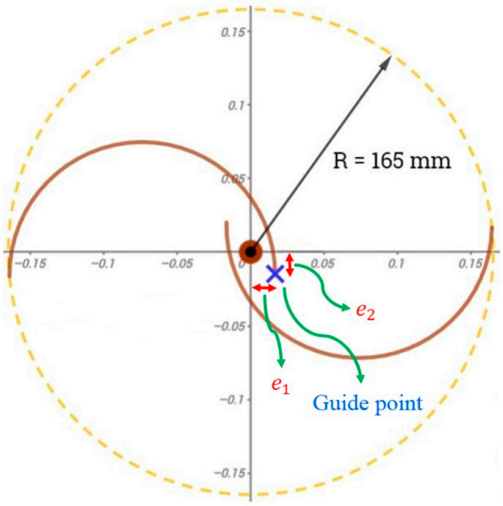

Figure 3. Schematic diagram. The overlap ratio is defined separately for the horizontal and vertical position by transferring the guide point in the Cartesian coordinate in two dimensions.

The wind speed suitable for the current simulations is considered based on the geographic atlas of wind speed in Iran (Figure 4). According to Figure 4, for the average altitude of 50 m in 2016, the appropriate and accessible wind speeds that can be reconstructed based on these simulation conditions are between 6 and 9 m/s. In the present work, the maximum of this value, i.e., 9 m/s, is selected and the simulations are carried out accordingly [34]. The swept area in this article is 0.33 m^2, the thickness of the blade is considered to be 2 mm according to the validation work, and the diameter of the mid-shaft is 15 mm [23]. Simulations begin by examining horizontal overlap ratios. The overlaps of 0, ±0.1, ±0.25, and ±0.4 are investigated. Then, according to the results and values, the overlap ratios of ±0.05, ±0.15, and +0.2 are also studied to obtain the best possible ratio (Figure 5).

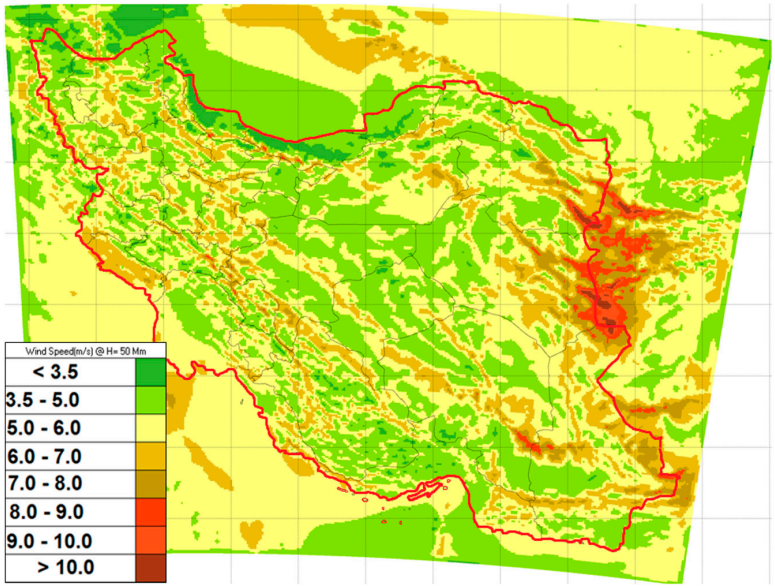

Figure 4. Wind Atlas of Iran for a height of 50 m, 2016, which is used to determine the acceptable wind speed for simulations [34].

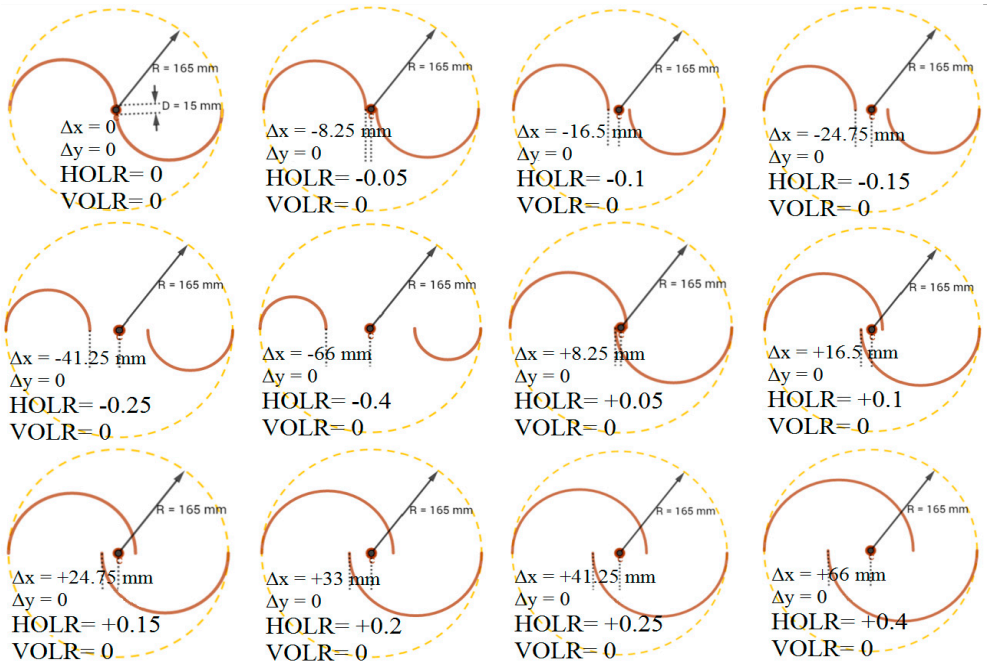

Figure 5. 2D schematic of rotors with investigated horizontal overlap ratios along the X-axis.

It may be mentioned that it is predictable that negative horizontal overlaps probably have a low efficiency, but they should be studied to check the amount of power difference in all cases. To understand whether the power reduction can be justified by a reduction in the amount of raw material consumption and production costs could be useful for future work.

2.1. Governing Equations and the Numerical Solution Method

The URANS equations are used for numerical solutions, in which the mass continuity and momentum conservation equations for the incompressible flow of Newtonian fluid are used.

A review of previous research revealed that in the examinations of wind turbines, the realizable K-ε turbulence model and the SST k-ω are preferred to the other turbulence models. This is mainly due to their satisfactory precision and speed of calculations and their highly precise solutions, respectively. In this work, the realizable K-ε turbulence model was selected with the following equations [22]:

$$\frac{\partial \rho}{\partial t}(\rho k) + \frac{\partial}{\partial x_j}(\rho k u_j) = \frac{\partial}{\partial x_j}\left[\left(\mu + \frac{\mu_t}{\sigma_k}\right)\frac{\partial k}{\partial x_j}\right] + G_k + G_b - \rho\varepsilon - Y_M + S_k \tag{4}$$

$$\frac{\partial \rho}{\partial t}(\rho \varepsilon) + \frac{\partial}{\partial x_j} = \frac{\partial}{\partial x_j}\left[\left(\mu + \frac{\mu_t}{\sigma_\varepsilon}\right)\frac{\partial \varepsilon}{\partial x_j}\right] + \rho C_1 - \rho C_2 \frac{\varepsilon^2}{k + \sqrt{\nu\varepsilon}} + C_{1\varepsilon}\frac{\varepsilon}{k}C_{3\varepsilon}G_b + S_\varepsilon \tag{5}$$

Here, G_k is the turbulence kinetic energy generation due to the gradient of average velocity; G_b is the turbulent kinetic energy generation due to the gradient of average buoyancy; and σ_k, and σ_ε are, respectively, the turbulent Prandtl number for k and ε equations. $C_{1\varepsilon}$, $C_{2\varepsilon}$, $C_{3\varepsilon}$, and C_μ are constants, and S_k and S_ε are source terms. Y_M is the effect of changing the expansion in compressible turbulence to a total dissipation rate, which is defined as

$$Y_M = 2\rho\varepsilon\frac{k}{\gamma RT} \tag{6}$$

and C_1 is defined as

$$S = \sqrt{2S_{ij}S_{ij}} \quad , \quad \eta = S\frac{k}{\varepsilon} \quad , \quad C_1 \quad = \max\left[0.43, \frac{\eta}{\eta + 5}\right] \tag{7}$$

In a wind turbine, the most important parameters in displaying the output efficiency of the system are the torque and output power. In the present work, with respect to these two parameters, the results are compared and analyzed. The non-dimensional results are expressed as torque and power coefficients. Their equations are as follows:

$$C_m = T/\left[(1/2)\rho A R U^2\right] \tag{8}$$

$$Cp = P/\left[(1/2)\rho A U^3\right] \tag{9}$$

T is the produced torque, A is the swept area in front of the wind stream, R is the rotor radius, U is the free stream velocity, and P is the output power.

Another dimensionless parameter which is used in wind turbine analysis is the tip speed ratio (TSR) and is defined as (12)

$$\lambda = \frac{R\omega}{U} \tag{10}$$

where ω is the rotational speed.

2.2. Mesh and Boundary Layers

The sliding mesh method is used to mesh the solution area. This consists of two fixed and rotating regions. Both areas are divided by triangle meshes (Figure 6). In order to eliminate the effects of walls

and independence from the solution domain, according to Mohamed et al. [23], the size of the sides of the constant area needs to be 25 times larger than the diameter of the rotor. Additionally, the diameter of the rotating zone has to be 1.25 times larger than the diameter of the turbine rotor. The length of the sides of the constant area was 8250 mm and the diameter of the rotating zone was 412.5 mm. The element size varied in different parts of the blade, and this value increased at the edges and sharp angles of 0.4 and on flat surfaces up to about 1 mm. Around the rotor and shaft, an inflation mesh with 15 to 20 layers was used to consider the walls effects. As a result of this fine meshing, the Y^+ value on the rotor blades was always less than 2.5.

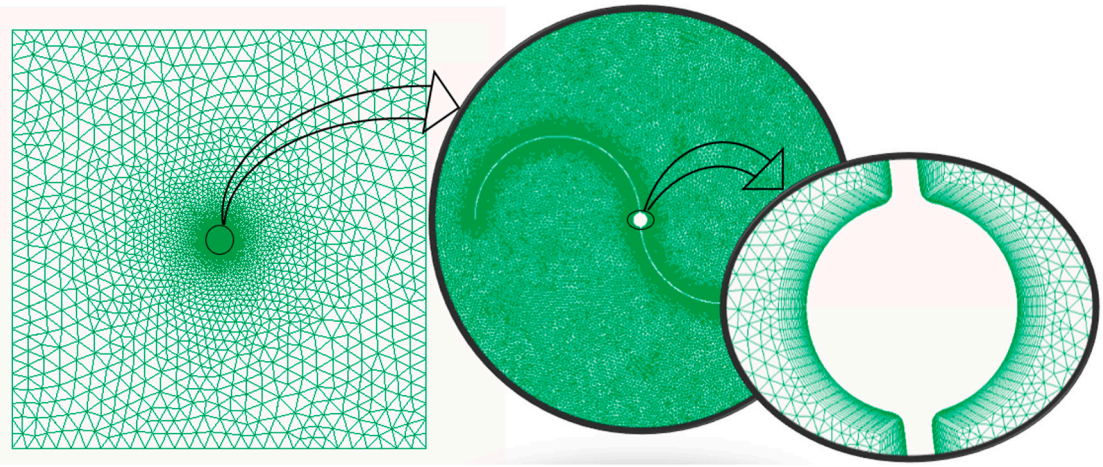

Figure 6. Triangular grid with 15 layers of inflation for a rotor with a horizontal overlap ratio (HOLR) of 0 and vertical overlap ratio (VOLR) of 0.

Given the physical conditions of the problem, the inlet boundary was assigned an inlet velocity, the outlet boundary was assigned an outlet pressure, the slide walls boundary was assigned a non-slip wall, and the rotor was assigned a non-slip wall.

3. Results and Discussion

In order to investigate the mesh independency, a criterion of overlap ratios is considered. For this purpose, the size of the elements on the blades and the interface between zones, the number of elements of cells was changed from 5400 to 730,000 (Figure 7). The mesh independence results showed that as the number of cells increases by more than 70,000, the gradient of the torque coefficient variation curve relative to the number of cells reaches approximately zero, so it was considered that a grid with 70,000 of cells would be appropriate. An examination of the results shows that when the number of cells is between 70,000 and 90,000 for different overlap ratios, acceptable responses will be achieved. It should be noted that the expression of a range for a mesh is due to the fact that for different geometries, the number of cells is slightly different. Meanwhile, considering the size of larger negative overlaps, the number of cells also decreases. Torque coefficients were recorded after two complete revolutions to ensure that the air flow was stable.

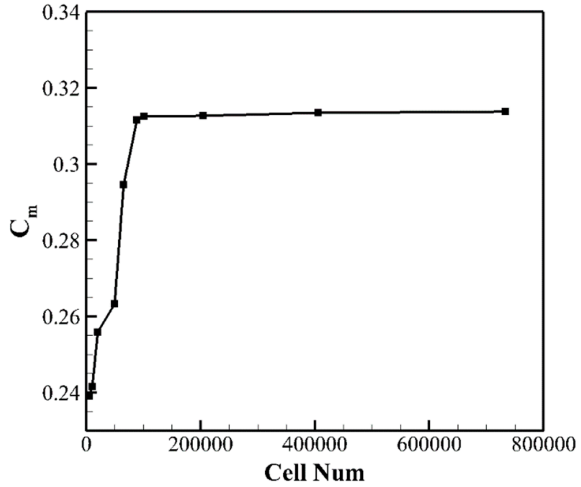

Figure 7. The mesh independency was investigated by changing the number of cells from 5400 to 730,000.

Validation was carried out according to the article by Mohamed et al. [23] at the wind speed of 10 m/s using the same turbulence models, where the validation diagrams related to the reference torque and the present work were compared. With a slight error, validation was achieved. The average error was found to be 3.73% (Figure 8). The difference in results could be because of the differences in meshing, the constant of the turbulence model, and uncertain environmental conditions, which are considered in the numerical simulations.

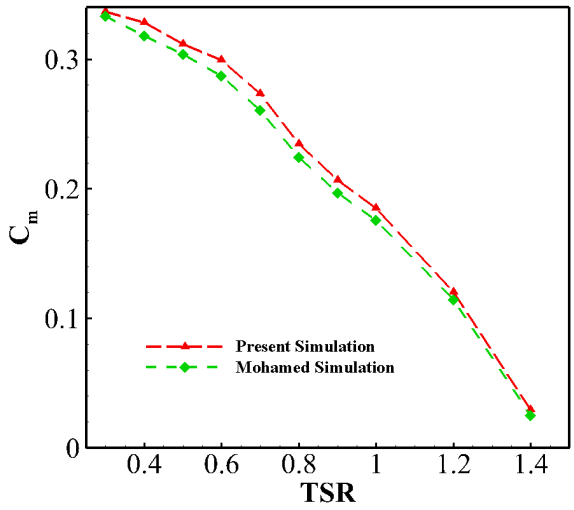

Figure 8. Validation of the numerical solution with Mohamed's results for U = 10 m/s.

After analyzing the horizontal overlap ratios, while the vertical overlap ratio was zero, the torque and power coefficients were obtained according to Figure 9. This shows that the horizontal overlap has a significant effect on the rotor performance. In horizontal–positive overlaps, the torque coefficients have higher values for lower TSRs. At the horizontal overlap ratio of +0.15, the maximum torque coefficient with the value of 0.4 is obtained at TSR = 0.25.

By increasing the tip speed ratios, in a range of TSR from 0.55 to 0.9, geometries with horizontal overlaps close to zero produce slightly higher torque coefficients compared to other horizontal overlaps. At values above a TSR of 0.9, the maximum torque coefficient is obtained at the horizontal overlap ratio of +0.15. The maximum produced power coefficient with an approximate value of 0.18 is related to zero overlap at the tip speed ratio of 0.7. However, the problem of the configuration with a slight overlap is a faster drop than the positive overlaps, due to the increase of the dimensionless TSR parameter.

This is what happens for the positive overlaps at slower rates. The reason for this is the presence of an overlap distance and steering return flow from the concave section of the backward blade to the convex section of the forward blade. This reduces the negative pressure produced by the Coanda flow, i.e., the tendency of a fluid jet to stay attached to a convex surface on the concave section of the forward blade. At negative overlap ratios, due to the absence of compensation for the negative pressure behind the forward blade, the torque coefficient and power coefficient show lower values. Accordingly, among horizontal overlaps, the value of +0.15 is suggested due to the higher efficiency for the wider range of tip speed ratios.

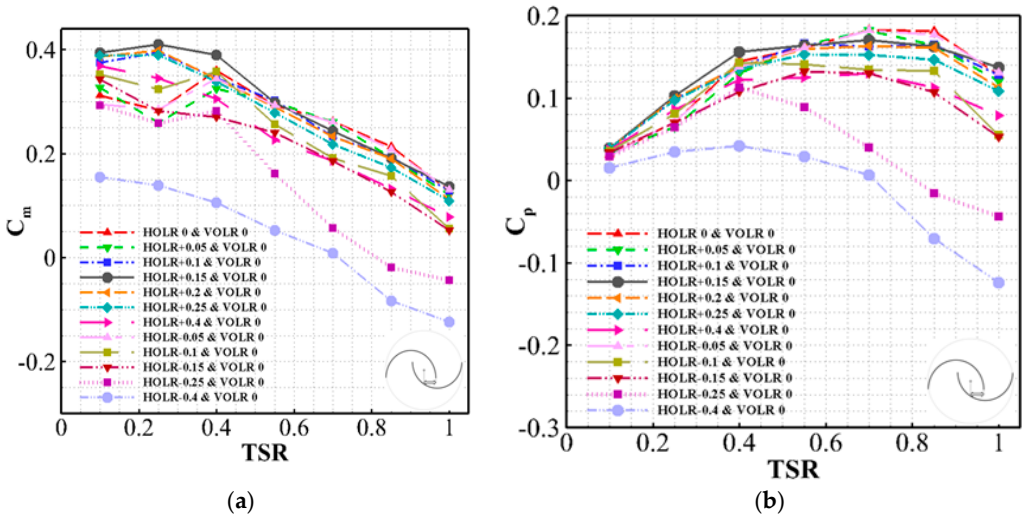

Figure 9. (**a**) Torque and (**b**) power coefficients obtained at different horizontal overlaps for a vertical overlap ratio (VOLR) of 0.

After choosing the optimal horizontal overlap ratio point, i.e., HOVR = +0.15, the variations of the vertical overlap ratio were investigated. For this, at first, the vertical overlap intervals ±0.1 and ±0.2 were checked and then, according to the resulting values, the overlaps ±0.05 and −0.15 were checked (Figure 10).

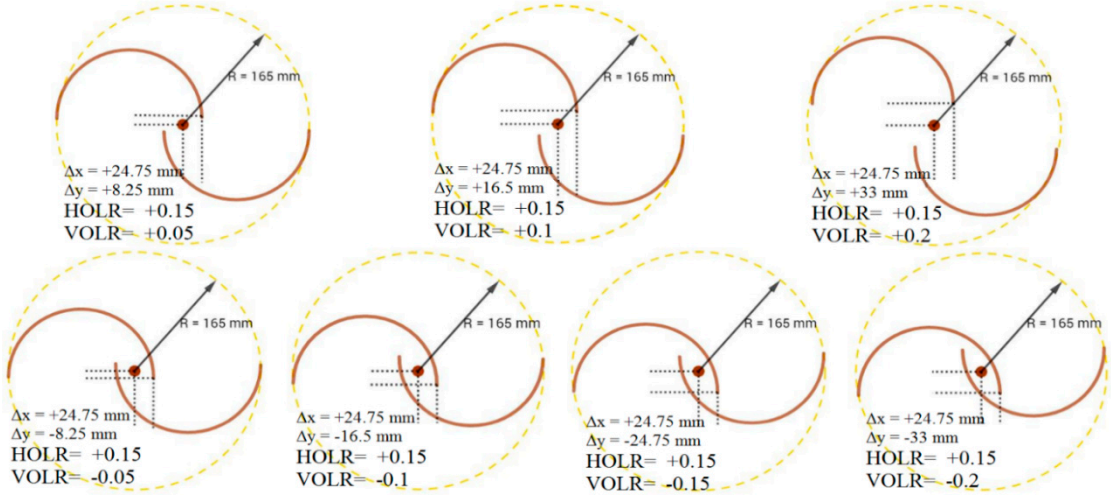

Figure 10. 2D schematic of rotors with investigated vertical overlap ratios along the Y-axis for a constant horizontal overlap ratio (HOLR) of +0.15.

The torque and power coefficients are shown in Figure 11. According to this figure, the vertical overlap ratio has a significant effect on the rotor performance. The torque coefficients have better

performances for lower tip speed ratios in negative vertical overlaps, reaching their optimal point at the overlap ratio of −0.1. Additionally, the highest drops are related to negative horizontal overlaps that do not have the ability to use return flow. Furthermore, the shorter the cord length of the blade becomes, the more effective it can be. The lowest efficiency is related to HOLR = 0 and VOLR = −0.4.

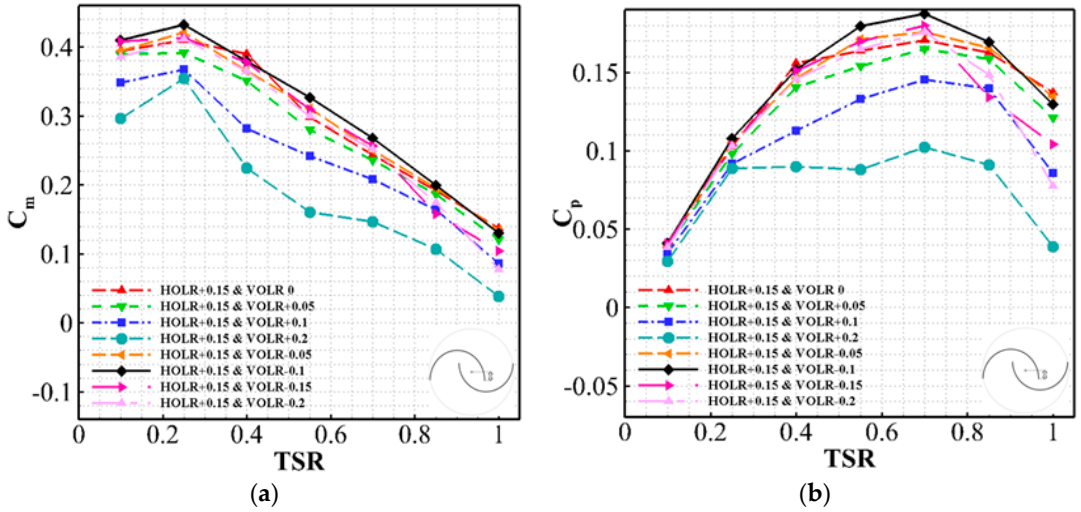

Figure 11. (**a**) Torque and (**b**) power coefficients obtained at different vertical overlap ratios along the Y-axis when the horizontal overlap ratio (HOLR) is +0.15.

The torque and power coefficient diagrams show that as the blades become farther away from each other in the vertical direction, the flow steering decreases sharply over the blade overlap, which is also observed when the blades are located at a very close distance to each other.

The power and torque coefficients of the base state with zero overlap, optimal overlap in the horizontal state, and the overall optimal overlap diagrams are shown in Figure 12. Only for a TSR of 0.85 is the zero overlap a little better. At the remaining TSRs, the rotor produces higher torque and power coefficients with HOLR = +0.15 and VOLR = −0.1 coordinates. For further consideration, a comparison of the average values is presented in Table 1.

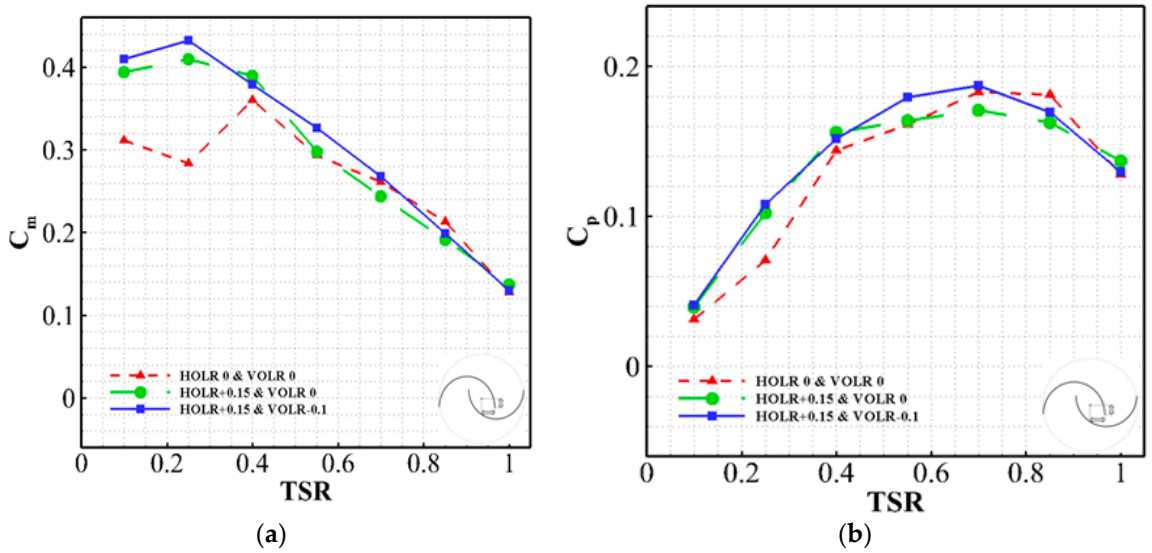

Figure 12. Variations trend and relative improvement of (**a**) torque and (**b**) power coefficients in three states of zero overlap ratio, optimal overlap ratio in horizontal investigation, and overall optimal overlap ratio.

Table 1. Comparison of the zero overlap ratio and optimal mode at horizontal and overall overlap ratios.

	HOLR = 0 VOLR = 0	HOLR = +0.15 VOLR = 0	HOLR = +0.15 VOLR = −0.1	% Increase with Regard to Horizontal Overlap Ratio Optimization	% with Regard to Overall Overlap Ratio Optimization
Average C_m	0.264	0.295	0.306	11.5	15.8
Average C_p	0.128	0.133	0.138	3.7	7.5

Regarding the optimization, the improvement percentage of the average C_m in the horizontal overlap state is 11.5%, and in the vertical overlap state, it is 16%, when compared to the base state with a zero overlap ratio. The improvement percentage in the average C_p, however, is less pronounced. Its increment in the most optimized horizontal overlap state is 3.7%, and in the best vertical overlap state, it is 7.5%, when compared to the same base state.

Given the similarity of the variations of the speed contours at different overlap ratios toward the TSR and the high number of contours, only the TSR of 0.4 is selected and presented in Figure 13 to observe the variation trend. The most obvious factor in these contours is the effect of overlaps on the utilization of the return flow from the concave section. As can be seen, steering the return flow reduces the pressure difference caused by the Coanda flow behind the forward blade. This, in return, results in an increase in the turbine efficiency.

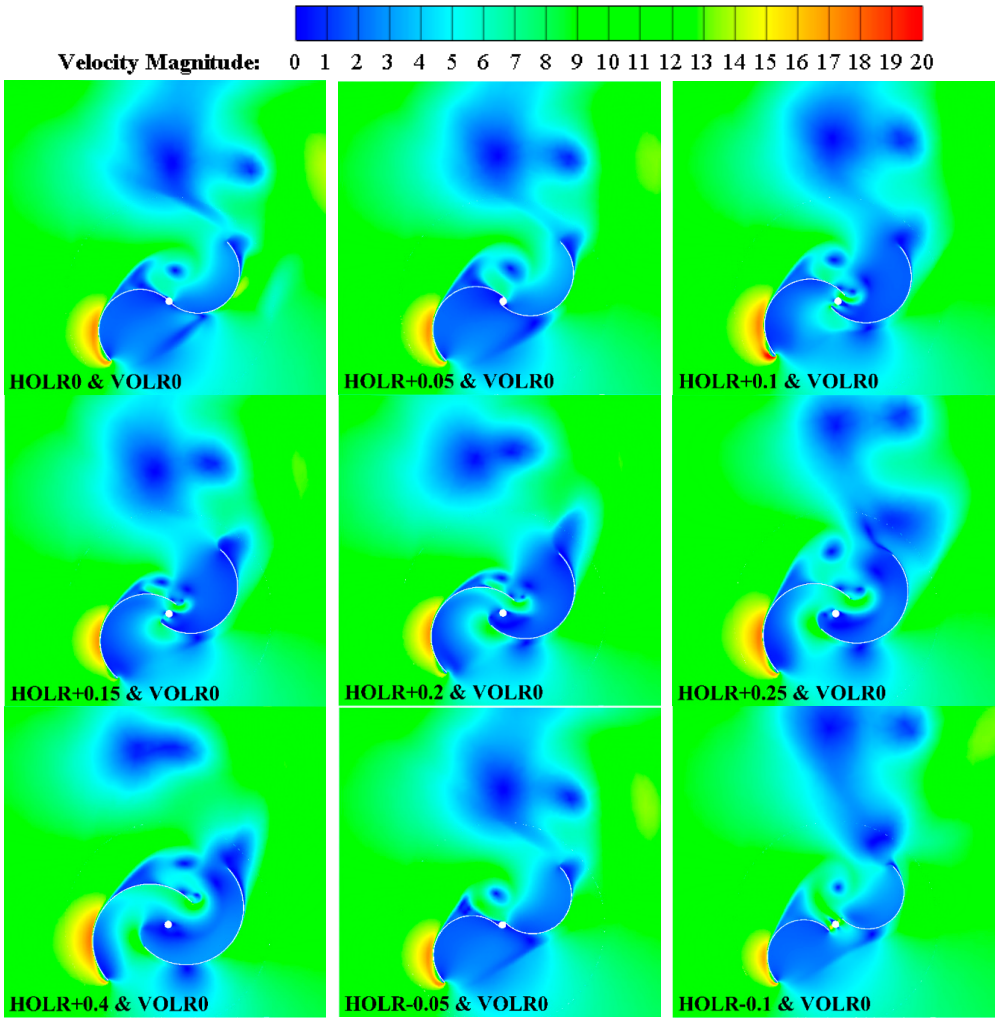

Figure 13. *Cont.*

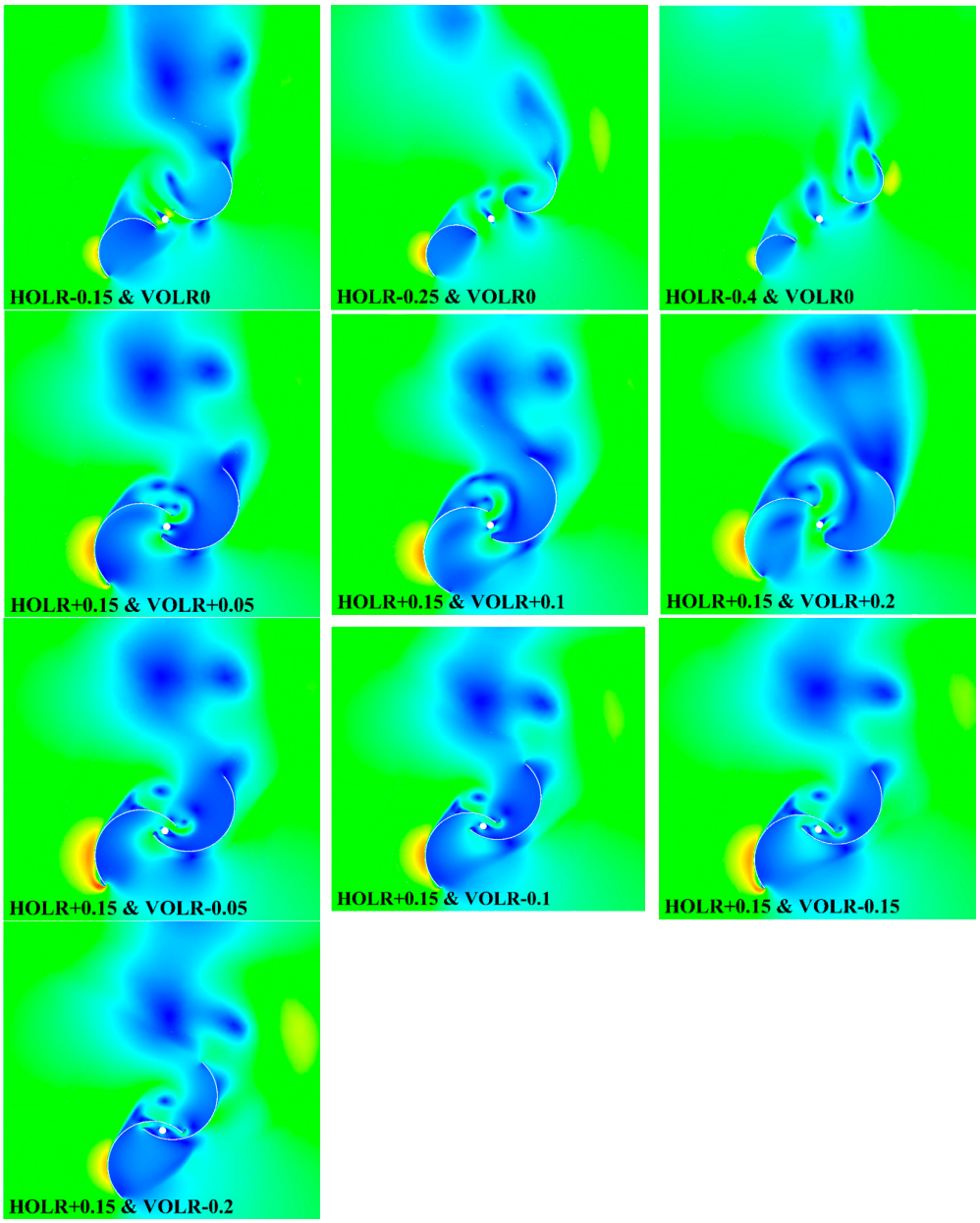

Figure 13. Velocity contours at different overlap ratios to display the gradient of velocity around the rotor for U = 9 m/s and the tip speed ratio (TSR) of 0.4.

The velocity contours show a growth of the vortex region independent of the tip speed ratio at the higher overlap ratios and near the positive overlap section. This indicates a deterioration of the aerodynamic efficiency at high tip speed ratios. The reason for this is due to the increase in the distance between the two blades, meaning that the return flow is scattered and does not properly hit the surface of the driving blade. Furthermore, the Torque coefficient variation graphs with time, during a cycle of rotor rotation, in the negative horizontal overlap state, indicate an extreme disturbance which results in system efficiency degradation. In fact, the system cannot achieve a trend with constant periodicity, which is one of the weak points of these geometries. With regard to the velocity contours, inside the overlap area, the return flow becomes turbulent by hitting the shaft, preventing the steered flow from fully colliding with the forward blade, thereby reducing the efficiency to a certain extent. By increasing the horizontal overlap angle, the effect of the shaft reduces, and this can have a positive effect on the system, but on the other hand, increasing the overlap distance reduces the efficiency. Therefore,

to achieve the optimal state, the outcome of these two parameters must be considered. All things considered, the rotor with a horizontal overlap of +0.15 and vertical overlap of −0.1 is a suitable option, especially at low tip speed ratios. Of course, it should be kept in mind that the Savonius rotors often operate at low tip speed ratios, which also indicates the efficiency of the geometry chosen.

4. Conclusions

In this study, a typical Savonius turbine with a constant diameter of the rotor was studied, where the variation of the overlap ratios in both horizontal and vertical directions was considered. In this paper, simulations were carried out by using the computational fluid dynamics (CFD) and solving the URANS equations and realizable K-ε turbulence model. The results showed that at near zero and positive horizontal overlap ratios, a relatively higher efficiency than that of the other states could be achieved. In fact, for lower tip speed ratios, the rotor with an overlap ratio of +0.15 produces a higher torque ratio and is more efficient in a wider range of tip speed ratios. Therefore, it was selected as the optimal horizontal overlap. In the next step, at this optimal point, vertical overlaps were investigated. Among these overlaps, the value of −0.1 showed the best torque and power coefficients. As a result, a rotor with a horizontal overlap ratio of +0.15 and vertical overlap ratio of −0.1 was selected as the optimal model. The improvement percentage in the average C_m in the horizontal overlap state, was 11.5%, and in the vertical overlap state, was 16%, when compared to the base state with zero overlap. Additionally, the improvement percentage in the average C_p in the horizontal overlap state was 3.7%, and in the vertical overlap state, was 7.5%, when compared to the same base state.

This article is a part of an ongoing project. In the next step, this optimal blade application will three-dimensionally examine an oscillating water columns (OWC) system. Finally, the effect of tensile forces on the rotor's structure will be investigated by using FSI simulation so that the information obtained can be used to select the raw materials and manufacture the rotor.

Author Contributions: Conceptualization, M.E., R.S., and R.A.; methodology, M.E., R.S., R.A., and M.S.S.; software, M.E.; validation, M.E.; formal analysis, M.E., R.S., R.A., and M.S.S.; investigation, M.E.; resources, R.S. and R.A.; data curation, M.E., R.S., and R.A.; writing—original draft preparation, M.E., writing—review and editing M.E., R.S., R.A., and M.S.S.; visualization, M.E., R.S., and R.A.; supervision, R.S., R.A., and M.S.S.; project administration, R.S. and R.A.; funding acquisition, R.S.

Funding: This research received no external funding.

Acknowledgments: The Sea-Based Energy Research Group at Babol Noshirvani University of Technology is acknowledged for providing technical and administrative assistance.

Conflicts of Interest: The authors declare no conflict of interest.

Nomenclature

TSR (λ) [-]	Tip speed ratio
VAWT	Vertical axis wind turbine
CFD	Computational fluid dynamics
U [m/s]	Free stream velocity
A [m^2]	Rotor swept area (A = DH)
C_P	Power coefficient
C_m	Torque coefficient
HOLR	Horizontal overlap ratio
VOLR	Vertical overlap ratio
D	Rotor diameter
RANS	Reynolds Averaged Navier–Stokes

References

1. Alamian, R.; Shafaghat, R.; Miri, S.J.; Yazdanshenas, N.; Shakeri, M. Evaluation of technologies for harvesting wave energy in Caspian Sea. *Renew. Sustain. Energy Rev.* **2014**, *32*, 468–476. [CrossRef]

2. Ghasemian, M.; Ashrafi, Z.N.; Sedaghat, A. A review on computational fluid dynamic simulation techniques for Darrieus vertical axis wind turbines. *Energy Convers. Manag.* **2017**, *149*, 87–100. [CrossRef]
3. Roy, S.; Ducoin, A. Unsteady analysis on the instantaneous forces and moment arms acting on a novel Savonius-style wind turbine. *Energy Convers. Manag.* **2016**, *121*, 281–296. [CrossRef]
4. Sawin, J.L.; Sverrisson, F.; Seyboth, K.; Adib, R.; Murdock, H.E.; Lins, C.; Appavou, F.; Brown, A.; Chernyakhovskiy, I.; Epp, B.; et al. *Renewables 2017 Global Status Report*; REN21: Paris, France, 2013.
5. Mohammadi, M.; Lakestani, M.; Mohamed, M. Intelligent parameter optimization of Savonius rotor using artificial neural network and genetic algorithm. *Energy* **2018**, *143*, 56–68. [CrossRef]
6. Ajayi, O. Application of Automotive Alternators in Small Wind Turbines. Master's Thesis, Delft University of Technology, Delft, Netherlands, 2012.
7. Svorcan, J.; Stupar, S.; Komarov, D.; Peković, O.; Kostić, I. Aerodynamic design and analysis of a small-scale vertical axis wind turbine. *J. Mech. Sci. Technol.* **2013**, *27*, 2367–2373. [CrossRef]
8. Chong, W.-T.; Muzammil, W.K.; Wong, K.-H.; Wang, C.-T.; Gwani, M.; Chu, Y.-J.; Poh, S.-C. Cross axis wind turbine: Pushing the limit of wind turbine technology with complementary design. *Appl. Energy* **2017**, *207*, 78–95. [CrossRef]
9. Alamian, R.; Shafaghat, R.; Safaei, M.R. Multi-objective optimization of a pitch point absorber wave energy converter. *Water* **2019**, *11*, 969. [CrossRef]
10. Esmaeelpour, K.; Shafaghat, R.; Alamian, R.; Bayani, R. Numerical study of various geometries of breakwaters for the installation of floating wind turbines. *J. Nav. Archit. Mar. Eng.* **2016**, *13*, 27–37. [CrossRef]
11. Alamian, R.; Shafaghat, R.; Ketabdari, M.J. Wave simulation in a numerical wave tank, using BEM. *AIP Conf. Proc.* **2015**, *648*, 770008. [CrossRef]
12. Méndez, M.; Shadloo, M.; Hadjadj, A.; Ducoin, A. Boundary layer transition over a concave surface caused by centrifugal instabilities. *Comput. Fluids* **2018**, *171*, 135–153. [CrossRef]
13. Ducoin, A.; Shadloo, M.; Roy, S. Direct numerical simulation of flow instabilities over Savonius style wind turbine blades. *Renew. Energy* **2017**, *105*, 374–385. [CrossRef]
14. Shikha; Bhatti, T.; Kothari, D. Early development of modern vertical and horizontal axis wind turbines: A review. *Wind Eng.* **2005**, *29*, 287–299. [CrossRef]
15. Wenehenubun, F.; Saputra, A.; Sutanto, H. An experimental study on the performance of Savonius wind turbines related with the number of blades. *Energy Procedia* **2015**, *68*, 297–304. [CrossRef]
16. Roy, S.; Saha, U.K. Wind tunnel experiments of a newly developed two-bladed Savonius-style wind turbine. *Appl. Energy* **2015**, *137*, 117–125. [CrossRef]
17. Tahani, M.; Rabbani, A.; Kasaeian, A.; Mehrpooya, M.; Mirhosseini, M. Design and numerical investigation of Savonius wind turbine with discharge flow directing capability. *Energy* **2017**, *130*, 327–338. [CrossRef]
18. Lee, J.-H.; Lee, Y.-T.; Lim, H.-C. Effect of twist angle on the performance of Savonius wind turbine. *Renew. Energy* **2016**, *89*, 231–244. [CrossRef]
19. Roy, S.; Das, R.; Saha, U.K. An inverse method for optimization of geometric parameters of a Savonius-style wind turbine. *Energy Convers. Manag.* **2018**, *155*, 116–127. [CrossRef]
20. Wang, Y.-F.; Zhan, M.-S. 3-Dimensional CFD simulation and analysis on performance of a micro-wind turbine resembling lotus in shape. *Energy Build.* **2013**, *65*, 66–74. [CrossRef]
21. Müller, G.; Chavushoglu, M.; Kerri, M.; Tsuzaki, T. A resistance type vertical axis wind turbine for building integration. *Renew. Energy* **2017**, *111*, 803–814. [CrossRef]
22. Roy, S.; Saha, U.K. Computational study to assess the influence of overlap ratio on static torque characteristics of a vertical axis wind turbine. *Procedia Eng.* **2013**, *51*, 694–702. [CrossRef]
23. Mohamed, M.; Janiga, G.; Pap, E.; Thévenin, D. Optimal blade shape of a modified Savonius turbine using an obstacle shielding the returning blade. *Energy Convers. Manag.* **2011**, *52*, 236–242. [CrossRef]
24. Hayashi, T.; Li, Y.; Hara, Y. Wind tunnel tests on a different phase three-stage Savonius rotor. *JSME Int. J. Ser. B Fluids Therm. Eng.* **2005**, *48*, 9–16. [CrossRef]
25. Rizzo, F.; Caracoglia, L. Examining wind tunnel errors in Scanlan derivatives and flutter speed of a closed-box. *J. Wind Struct.* **2018**, *26*, 231–251.
26. Tian, W.; Mao, Z.; An, X.; Zhang, B.; Wen, H. Numerical study of energy recovery from the wakes of moving vehicles on highways by using a vertical axis wind turbine. *Energy* **2017**, *141*, 715–728. [CrossRef]
27. Rogowski, K. Numerical studies on two turbulence models and a laminar model for aerodynamics of a vertical-axis wind turbine. *J. Mech. Sci. Technol.* **2018**, *32*, 2079–2088. [CrossRef]

28. Ferrari, G.; Federici, D.; Schito, P.; Inzoli, F.; Mereu, R. CFD study of Savonius wind turbine: 3D model validation and parametric analysis. *Renew. Energy* **2017**, *105*, 722–734. [CrossRef]
29. Jin, X.; Wang, Y.; Ju, W.; He, J.; Xie, S. Investigation into parameter influence of upstream deflector on vertical axis wind turbines output power via three-dimensional CFD simulation. *Renew. Energy* **2018**, *115*, 41–53. [CrossRef]
30. Fujisawa, N. On the torque mechanism of Savonius rotors. *J. Wind Eng. Ind. Aerodyn.* **1992**, *40*, 277–292. [CrossRef]
31. Kumbernuss, J.; Chen, J.; Yang, H.; Lu, L. Investigation into the relationship of the overlap ratio and shift angle of double stage three bladed vertical axis wind turbine (VAWT). *J. Wind Eng. Ind. Aerodyn.* **2012**, *107*, 57–75. [CrossRef]
32. Arriving at the optimum overlap ratio for an elliptical-bladed Savonius rotor. In *ASME Turbo Expo 2017: Turbomachinery Technical Conference and Exposition*; Alom, N.; Saha, U.K., Eds.; American Society of Mechanical Engineers: New York, NY, USA, 2017.
33. Roy, S.; Saha, U.K. Review of experimental investigations into the design, performance and optimization of the Savonius rotor. Proceedings of the Institution of mechanical engineers, part A. *J. Power Energy* **2013**, *227*, 528–542. [CrossRef]
34. Atlas Iw. Available online: http://www.satba.gov.ir/fa/regions/windatlas (accessed on 17 June 2018).